# Picosecond response of photoexcited GaAs in a uniform electric field by Monte Carlo dynamics

G. M. Wysin, D. L. Smith, and Antonio Redondo
*Los Alamos National Laboratory, The University of California, Los Alamos, New Mexico 87545*
(Received 22 February 1988)

The transient electrical response of GaAs photoexcited by a subpicosecond pulse, in the presence of a uniform biasing electric field, has been studied with use of a Monte Carlo calculation. Noninteracting electron transport is considered, using the three-valley model for the conduction band. Scattering from acoustic, optical, and intervalley phonons is included. The valence-band dispersion relations and valence- to conduction-band momentum matrix elements needed to treat the optical absorption were obtained from a full-zone $\mathbf{k}\cdot\mathbf{p}$ calculation. The optical absorption has been given a realistic treatment by including an effective energy linewidth resulting from the combination of the Fourier transform of the driving pulse, electron-phonon scattering, and the effect of the applied electric field. The average electron velocity is found to overshoot its steady-state value only if the electric field is larger than a critical value which increases with the photon energy. For example, these calculations indicate that at 5.0 kV/cm overshoot occurs for a photon energy of 1.5 eV but not for 1.7 eV. Velocity overshoot is seen to occur when the steady-state average electron energy (for the given applied field) is larger than the average electron energy of the initial photoexcited distribution. The regime of applied field and photon energy necessary for overshoot is mapped out.

## I. INTRODUCTION

Design of semiconductor devices with desired high-speed properties requires an understanding of how the microscopic *dynamics* of carrier transport results in a particular electrical response. The transient response of a semiconductor is a direct consequence of the relaxation of the carrier distribution towards its steady state. The relaxation depends on the interactions of the carriers with the lattice and with each other, as well as on the details of the band structure. An accurate microscopic model of the carriers' dynamics therefore can be a very useful predictive tool. The Monte Carlo (MC) method[1-5] can be employed in the accurate calculation of individual semiclassical electron (and hole) trajectories and thus, can ultimately give the macroscopic response. At the same time its appeal to physical intuition and direct interpretation make it ideally suited to these distribution relaxation problems.

Laser excitation provides a convenient method for suddenly changing the carrier distribution and then following the relaxation. Current experimental techniques allow for measurement of electrical transients in semiconductors on the subpicosecond time scale. Experiments have been performed in which a colliding-pulse, mode-locked (CPM) laser is used to produce a train of pulses that have durations of about 100 fs and energies of 2.0 eV. The beam of pulses is split into two beams, with a timing relationship that can be precisely varied. One beam is used to photogenerate electron-hole pairs in an electrically biased semiconductor sample, and the second beam is used in the temporal sampling of the electrical response.[6-8] The sampling can be performed either with a short response-time photoconductor or with an electrooptic polarizing material.

The CPM lasers that have been used for such experiments are tunable only over a very narrow spectra range near 2.0 eV. However, experimental studies for a range of photon energies are needed to fully characterize photoconductive response, because the initial carrier distribution depends strongly on the photon energy. Experimental techniques to generate spectrally tunable subpicosecond pulses are becoming available.[9,10] To aid in the interpretation and understanding of these types of experiments, we present a MC calculation of the relaxation of the distribution for photoexcited GaAs in the presence of a uniform electric field. In particular, the dependence of the response on the photon energy will be determined.

The dynamics of carrier relaxation toward a steady-state distribution depends on the initial distribution and on the steady-state distribution. The initial distribution is determined by the characteristics of the laser pulse, principally the photon energy, and the steady-state distribution is determined by the electric field. In this paper we present a systematic series of Monte Carlo calculations of electron relaxation in GaAs. We consider the case in which the electrons are generated by a 100-fs optical pulse and the GaAs is biased by a uniform electric field. We investigate the dynamics of the electron relaxation as a function of the photon energy and the magnitude of the applied field.

Similar MC calculations[3] have been performed with a field, but using as initial condition the state with all carriers at rest at $\mathbf{k}=\mathbf{0}$. It is impossible to create this situation experimentally. Photoexcitation results in the initial carrier distribution occupying two or three shells in $\mathbf{k}$ space, one from each of the highest valence bands. For the $\mathbf{k}=\mathbf{0}$ initial condition, MC calculations predict that the transient average carrier velocity overshoots its steady-state value, sometimes by a large factor. The initial condition produced by photoexcitation, however, can lead to completely different results, such as a lack of any

 

overshoot feature. In this paper we determine the conditions on the photon energy and bias field for electron velocity overshoot to occur.

Our calculations indicate that an accurate determination of the photoexcited distribution (and therefore its average electron energy) is necessary for an accurate modeling of the electrical response. We find that velocity overshoot occurs only when the initial-state average electron *energy* is less than the steady-state value. The *initial* average energy is roughly proportional to the photon energy minus the band gap, and the *steady-state* average energy is a nonlinear function of the applied field, so that the presence of velocity overshoot is determined by the relative size of the photon energy compared with the field.

We have calculated the photoexcited distribution by using valence bands obtained from a full-zone $\mathbf{k}\cdot\mathbf{p}$ calculation, while using a nonparabolic effective-mass fit to the $\Gamma$ valley of the conduction band. The fitting procedure for the conduction band (as opposed to the full-zone $\mathbf{k}\cdot\mathbf{p}$ results) was used to be consistent with the description of the conduction band in terms of its $\Gamma$, $L$, and $X$ valleys in the MC calculation. In this way the scattering processes are easier to treat. Effects of an absorption linewidth have also been included, through use of the Maxwell-Bloch equations with a damping time $T_2$, applied to a light pulse with an electric field varying with time according to $\mathrm{sech}(t/\tau_0)$, where $\tau_0$ is a width parameter. In these calculations, the laser intensity is assumed to have a full width at half maximum (FWHM) of 100 fs, and photon energies will be considered from 1.5 to 2.2 eV. The time $T_2$ is determined in a self-consistent manner by the total carrier scattering rate and the applied electric field. Typically we will have $T_2 \ll \tau_0$ so the line shape will be Lorentzian with energy width varying as $1/T_2$. Because of the energy dependence of the scattering rates, the linewidths will be functions of both the electric field and the photon energy. For moderately large fields and photon energies, the widths can become as large as $\approx 100$ meV. We have found, however, that the net effect of this energy width for most cases of interest has been rather small.

To obtain the leading-order response behavior, a number of simplifying assumptions have been used. First of all, for the low number density limit, carrier-carrier interactions are excluded. This approximation is valid at low laser intensity. At room temperature, the photogenerated carrier density should not exceed about $10^{17}$ cm$^{-1}$. The electric field is assumed to be uniform. This latter condition may actually be difficult to satisfy experimentally. Device response calculations based on a macroscopic continuum model indicate that the response of a high resistivity photoconductor to a moderate intensity subpicosecond pulse involves a collapse of the electric field, due to the opposing directions of electron and hole drift.[11] Using low laser intensity, so that the photogenerated carrier density is small, minimizes the effects of the collapsing electric field.[11] We take into account only the transport of electrons, assuming that the lower drift velocity of the holes makes their contributions to the electrical response much smaller.[12] As mentioned above, the conduction band will be considered as composed of the valleys at points $\Gamma$, $L$, and $X$. This means that the process of drifting from the $\Gamma$ point over the energy peak and then into either the $L$ or $X$ valley is excluded. Typically the scattering rates increase strongly enough (moving up in the band) so that this process is improbable.

The band structure for GaAs as obtained from the full-zone $\mathbf{k}\cdot\mathbf{p}$ calculation is reviewed in Sec. II. Details of the model employed for the MC calculation, including the necessary scattering rate parameters and valley fitting constants, are discussed in Sec. III. Results of a steady-state transport calculation of GaAs are also given. In Sec. IV the details of how the photoexcited initial distribution was generated and how the linewidth was included are discussed. Results are presented in Sec. V for GaAs with fields up to 50 kV/cm and photon energies ranging from 1.5 to 2.2 eV. Our conclusions concerning the trends in the photoresponses are discussed in Sec. VI.

## II. BAND STRUCTURE FOR GaAs

It is straightforward to apply the $\mathbf{k}\cdot\mathbf{p}$ pseudopotential method to the GaAs band structure. The calculation was carried out by first using a basis of 113 plane-wave states, corresponding to reciprocal-lattice vectors of the zinc-blende structure with squared magnitudes of 0, 3,4, 8, 11, 12, 16, and 20 [in units of $(2\pi/a)^2$]. After diagonalization for $\mathbf{k}=0$, only the 27 lowest energy states are retained. The spin-orbit interaction is added at this point, with splitting parameters $\Delta_0=0.34$ eV and $\Delta_1=0.22$ eV, and the $54\times 54$ matrix is then diagonalized for a range of $\mathbf{k}$. Input to the calculation is through the pseudopotential form factors, which have been taken from Ref. 13, for 300 K. We modified these form factors slightly to those given in the caption of Fig. 1, in order to enforce the band gap to be 1.44 eV, and the splittings from $\Gamma$ to $L$ and from $\Gamma$ to $X$ to be 0.33 and 0.52 eV, respectively. The lattice spacing is taken to be $a=5.6533$ Å

The resulting band structure is shown in Fig. 1. An effective-mass fit to the $\Gamma$ valley of the conduction band gives $m^*/m_0\approx 0.077$, with a nonparabolicity parameter $\alpha\approx 0.8$ eV$^{-1}$. It is difficult to find a set of pseudopotential form factors that will produce an effective mass and nonparabolicity close to the accepted values of 0.063 and 0.69 eV$^{-1}$, respectively.[4] Correspondingly, heavy-hole and split-off hole masses are approximately 0.7 and 0.2, reasonably close to accepted values. Similarly we can estimate the resulting effective conduction-band masses near the $L$ and $X$ points. Taking these as ellipsoidal valleys, approximate longitudinal and transverse masses turn out to be $m_l^L/m_0 \approx 1.5$, $m_t^L/m_0\approx 0.12$, $m_l^X/m_0\approx 1.5$, and $m_t^X/m_0\approx 0.25$. These values were used in the fits to these valleys for the MC calculations. The major utility of this band-structure calculation, however, was in employing its valence bands for the photoabsorption calculation, and also in using the valence- to conduction-band momentum matrix elements for correctly weighting the allowed optical transitions. The conduction band ($\Gamma$ valley), however, was fitted with an effective mass of $0.063m_0$ and nonparabolicity of 0.69 eV$^{-1}$ for the photoabsorption calculation, in order to use the same

fit in the MC calculation and therefore to conserve energy correctly.

## III. MONTE CARLO MODEL AND STEADY-STATE RESULTS

The MC method as applied to transport in semiconductors has been described in Ref. 1. In the semiclassical approximation, drift of a carrier in the applied electric field is treated classically as smooth motion in a band, interrupted by quantum-mechanical scattering events that discontinuously change the carrier's wave vector **k**. The conduction band can be described in terms of the valleys at $\Gamma$ [$\mathbf{k}=(0,0,0)$], $L$ [$\mathbf{k}=(\frac{1}{2},\frac{1}{2},\frac{1}{2})2\pi/a$ and other symmetric points in the star of **k**] and $X$ [$\mathbf{k}=(1,0,0)2\pi/a$ and other symmetric points in the star of **k**], with intervalley phonon scattering making transitions between the valleys possible. The $L$ and $X$ valleys are taken to be ellipsoidal and nonparabolic. In this way, in an applied field the three $X$ valleys and four $L$ valleys become inequivalent for an arbitrary field direction, and effects of this **k**-space anisotropy are retained. There may be some dependence of the response on the field direction that cannot appear if all the valleys are taken to be spherical. This effect might be expected to be strongest for large electric fields. The ratios of transverse to longitudinal effective mass have been taken from the full-zone **k**·**p** calculation, and the density-of-states masses $m_d=(m_l m_t^2)^{1/3}$ have been fixed to values given in Ref. 4, which also was the source for the valley nonparabolicity parameters. Thus the dispersion within each valley is given by a relation

$$\varepsilon(k^*)=\varepsilon_0+\frac{1}{2\alpha}\left[-1+\left[1+4\alpha\frac{\hbar^2}{2m_0}(k^*)^2\right]^{1/2}\right], \quad (1)$$

where

$$(k^*)^2=\frac{m_0}{m_t}k_t^2+\frac{m_0}{m_l}k_l^2 . \quad (2)$$

Here $\varepsilon_0$ is the energy at the bottom of the valley, and $k_l$ and $k_t$ are the longitudinal and transverse components of **k** as measured in the valley, and $\alpha$ is the nonparabolicity parameter.

The electrons are assumed to scatter from acoustic, polar optic, nonpolar optic (only in the $L$ valley), and intervalley phonons. In the low number density limit we exclude carrier-carrier interactions. A fictitious "self-scattering" is also included, so that the time intervals between scattering events can be chosen from an exponential distribution. (See Ref. 1.) The interaction Hamiltonians for each type of scattering process and expressions for the scattering rates can be found in Refs. 1 and 2; coupling constants and phonon frequencies have been taken from Table I of Ref. 4. The total scattering rate due to real physical processes (excluding self-scattering) will depend on the valley as well as on the carrier energy. Measuring all energies relative to the energy at the $\Gamma$ point, the total scattering rates for GaAs at 300 K are shown in Fig. 2, including contributions of phonon emission and absorption processes.

For noninteracting electrons, a large number of single-electron trajectories can be generated, and then averages of time-dependent quantities can be made by averaging over all the trajectories. For each trajectory, the final **k** state after each scattering event and the times of the

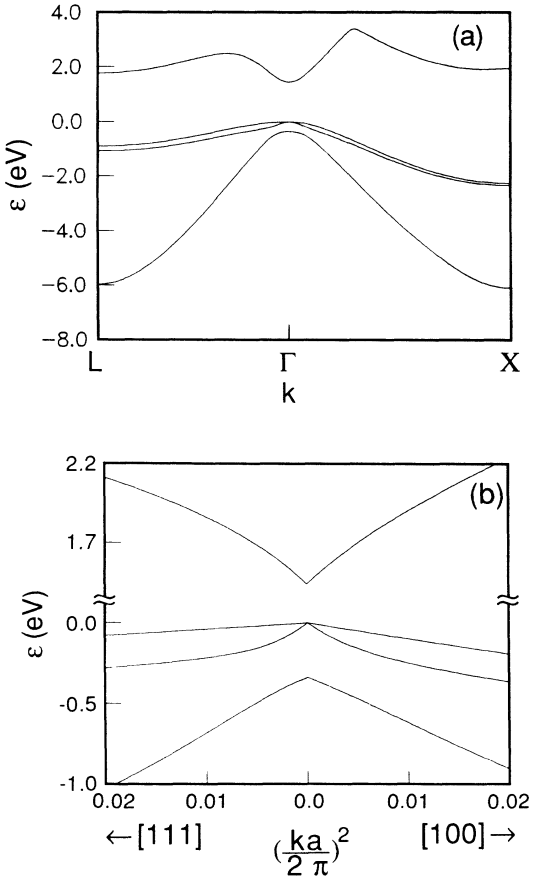


FIG. 1. GaAs band structure from the full-zone **k**·**p** calculation. In the notation of Ref. 13, the nonzero pseudopotential form factors, in Rydbergs, were $V_3^S=-0.237$, $V_3^A=0.07$, $V_4^A=0.0496$, $V_8^S=0.01$, $V_{11}^S=0.0628$, and $V_{11}^A=0.01$. (a) Shown over the whole zone vs $k$. (b) Region near $k=0$ vs $k^2$, to exhibit the deviations from parabolic bands.

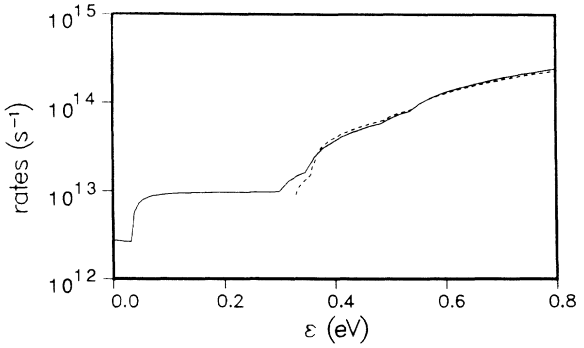


FIG. 2. Energy dependence of the total electron-phonon scattering rates, including acoustic, optical, and intervalley phonons. The curves correspond to an electron in the $\Gamma$ valley (——), $L$ valley (— — —), and $X$ valley (· · · ·).

events are enough to reconstruct the electron's $\mathbf{k}$ state at any desired time. For the scattering time intervals to belong to an exponential distribution, they are chosen with a random number $0<r<1$ by

$$\Delta t_s=\Gamma_0^{-1}\ln(r) \quad \text{where } \Gamma_0=\Gamma_{\text{phys}}+\Gamma_{\text{ss}} . \tag{3}$$

The constant $\Gamma_0$ is a scattering rate chosen to be greater than the sum of the rates of all the real physical processes, $\Gamma_{\text{phys}}$, and it is assumed that the electron energy never exceeds some chosen maximum value. The difference $\Gamma_0-\Gamma_{\text{phys}}(\varepsilon)$ gives the self-scattering rate $\Gamma_{\text{ss}}$, at the energy $\varepsilon$. When a self-scattering event occurs, the electron's final state is set equal to its initial state, and it continues to drift in the field as if no scattering occurred. The term "self-scattering" is a misnomer; a better name for it might be "nonscattering."

Between scattering events, the equation of motion is

$$\hbar\dot{\mathbf{k}}=q\mathbf{E} , \tag{4}$$

where $q$ is the charge and $\mathbf{E}$ is the applied field. At each scattering time the type of scattering process is chosen randomly but according to the relative probabilities of each of the allowed processes, using a random number generator. The random number generator is also used to choose an allowed final state, from those consistent with conservation of energy and momentum. For scattering from optical photons, choosing from the allowed states is relatively easy because the phonon frequency is fixed. For acoustic phonons the choice is more difficult and a "rejection technique" for choosing final states of the desired distribution is used (as in Ref. 1).

The time-dependent response quantities of most interest are the average velocity (or current), the average carrier energy, and the relative populations of the valleys. This velocity is determined by

$$\mathbf{v}=\frac{1}{\hbar}\frac{\partial\varepsilon}{\partial\mathbf{k}} . \tag{5}$$

For the steady-state case, time averages of these quantities can be easily calculated, and fewer electrons are needed to get small statistical errors than are needed for time-dependent problems. As an example, we have reproduced the calculation of the steady-state conduction in GaAs at 300 K, using the trajectories of 400 electrons for 100 ps. The beginning 20 ps of each trajectory was discarded. Results for the average velocity and energy versus the applied field (in the [100] direction) are shown in Fig. 3. The initial condition consisted of all electrons starting at $\mathbf{k}=0$, with averages formed from the data after the initial transient passed. The carrier energy tends to saturate because the scattering rates, which increase with energy, compete against the applied field, tending to prevent the energy from increasing. The energy versus field curve will be relevant for estimating the velocity overshoot regime for the time-dependent photoexcited transport problem.

## IV. GENERATION OF THE PHOTOEXCITED INITIAL DISTRIBUTION

We consider a laser pulse with vector potential varying as

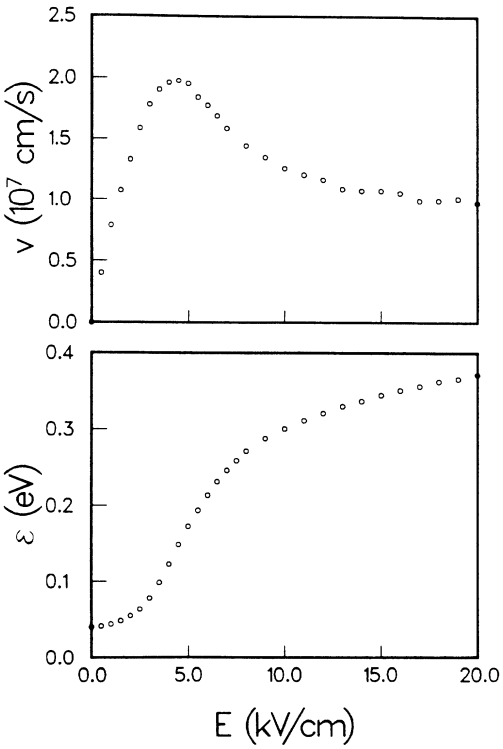


FIG. 3. Results of a steady-state MC calculation for GaAs at 300 K. The average electron velocity and energy were obtained by simulating the trajectories of 400 electrons for 100 ps, after discarding first 20 ps containing the transient effects of the $\mathbf{k}=\mathbf{0}$ initial condition.

$$\mathbf{A}(t)=A_0\hat{\boldsymbol{\varepsilon}}e^{i\omega_0 t}\operatorname{sech}(t/\tau_0) , \tag{6}$$

with amplitude $A_0$, polarization unit vector $\hat{\boldsymbol{\varepsilon}}$, center frequency $\omega_0$, and envelope width parameter $\tau_0$. (For this envelope, the laser intensity FWHM is $1.76\tau_0$). If effects of the absorption linewidth due to damping are excluded, and also $\omega_0\tau_0\gg1$, then the rate for a transition from a valence-band state $v_{\mathbf{k}}$ to a conduction-band state $c_{\mathbf{k}}$ is given in the dipole approximation by Fermi's golden rule,

$$W=\frac{2\pi}{\hbar}|\langle c_{\mathbf{k}}|\mathcal{H}_{\text{int}}|v_{\mathbf{k}}\rangle|^2\delta(\varepsilon_c-\varepsilon_v-\hbar\omega_0) , \tag{7}$$

with interaction Hamiltonian

$$\mathcal{H}_{\text{int}}=\frac{e}{m_0c}\mathbf{A}\cdot\mathbf{p} . \tag{8}$$

Here the envelope slowly modulates the transition rate. The general case with damping will be considered in more detail below. States in $\mathbf{k}$ space are chosen satisfying the $\delta$ function, with the conduction band described by Eq. (1) and the valence-band dispersion $\varepsilon_v(k)$ derived from the full-zone $\mathbf{k}\cdot\mathbf{p}$ calculation. The $\delta$ function defines an equi-energy surface in $\mathbf{k}$ space. After choosing a random direction in $\mathbf{k}$ space, the magnitude of $\mathbf{k}$ for the transition from a chosen valence band is found numerically. When computing averages, the subsequent MC trajectory of the electron created at that $\mathbf{k}$ is then weighted by the momentum matrix element $|\langle c_{\mathbf{k}}|\hat{\boldsymbol{\varepsilon}}\cdot\mathbf{p}|v_{\mathbf{k}}\rangle|^2$. An initial distribution of electron states will be composed of

either two or three peaks, due to the two or three allowed valence- to conduction-band transitions, and they will have small energy widths caused by the angular dependence of the valence-band dispersion relations. For transitions from a given hole band, numerical integration of the transition rate over the equi-energy surface then gives the relative contribution of transitions from that hole band to the absorption. Initial electron states are thus created from the two or three allowed transitions with the appropriate relative numbers (as determined by these integrals involving the optical matrix elements). The total absorption coefficient $\alpha_{\text{abs}}$ and the contributions from the three transitions are shown in Fig. 4.

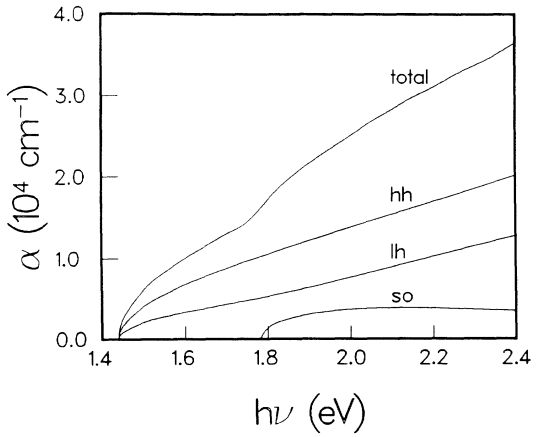


FIG. 4. Calculated GaAs absorption coefficient, as obtained by using optical matrix elements from the full-zone $\mathbf{k}\cdot\mathbf{p}$ calculation. The relative contributions from the three valence bands are indicated; these were applied to the generation of the photoexcited initial electron states.

Strictly speaking, Fermi's golden rule as given above should be used only in situations where the electron will not likely scatter during the laser pulse time interval. If the scattering rate is high enough, however, a linewidth is introduced due to the finite lifetime of the excited state. Similarly, an applied field also causes a finite lifetime and therefore a linewidth. The effects of both of these processes can be incorporated in terms of a damping time $T_2$ as a parameter for the Maxwell-Bloch (MB) equation. If the electron-photon interaction Hamiltonian is written in the form

$$\mathcal{H}_{\text{int}}=\gamma(\mathbf{k})a(t)\ , \tag{9}$$

with

$$\gamma(\mathbf{k})=\frac{eA_0}{m_0c}\langle c_{\mathbf{k}}|\hat{\boldsymbol{\varepsilon}}\cdot\mathbf{p}|v_{\mathbf{k}}\rangle\ ,$$
$$a(t)=2\cos(\omega_0 t)\operatorname{sech}(t/\tau_0)\ , \tag{10}$$

then the transition rate $w(t)$ is given by

$$w(t)=\frac{1}{\hbar}a(t)F(t)\ , \tag{11}$$

where $F(t)$ satisfies the MB equation in the form

$$\frac{d^2F}{dt^2}+\frac{2}{T_2}\frac{dF}{dt}+\left[\left[\frac{\Delta\varepsilon}{\hbar}\right]^2+\frac{1}{T_2^2}\right]F=\frac{2|\gamma|^2}{\hbar}\left[\frac{da}{dt}+\frac{a}{T_2}\right]. \tag{12}$$

Here $\Delta\varepsilon$ is the transition change in energy between valence and conduction bands, as in

$$\Delta\varepsilon=\varepsilon_c(\mathbf{k})-\varepsilon_v(\mathbf{k})\ . \tag{13}$$

Equation (12) can be solved by Fourier transforms. Performing the inversion by summing over the required poles produces the following expressions for the time-dependent transition rate: for $t<0$,

$$w(t)=\frac{4\tau_0|\gamma|^2}{\hbar^2}\operatorname{sech}(t/\tau_0)\sum_{n=0}^{\infty}(-1)^n\frac{t_n e^{(2n+1)t/\tau_0}}{(\Omega\tau_0)^2+t_n^2}\ , \tag{14}$$

$$t_n=(2n+1)+\frac{\tau_0}{T_2}\ , \tag{15}$$

and for $t>0$,

$$w(t)=\frac{4\tau_0|\gamma|^2}{\hbar^2}\operatorname{sech}(t/\tau_0)\left[-\sum_{n=0}^{\infty}(-1)^n\frac{\tilde{t}_n e^{-(2n+1)t/\tau_0}}{(\Omega\tau_0)^2+\tilde{t}_n^2}+\pi\frac{e^{-t/T_2}}{\cosh(2\beta)+\cos(2\alpha)}[\sin\alpha\sinh\beta\sin(\Omega t)+\cos\alpha\cosh\beta\cos(\Omega t)]\right], \tag{16}$$

$$\tilde{t}_n=(2n+1)-\frac{\tau_0}{T_2},\quad \alpha=\frac{\pi\tau_0}{2T_2},\quad \beta=\frac{\pi\Omega\tau_0}{2}\ , \tag{17}$$

where the detuning from resonance $\Omega$ is given by

$$\Omega=\frac{\Delta\varepsilon}{\hbar}-\omega_0\ . \tag{18}$$

Some typical curves of $w(t)$ for damping ratio $\tau_0/T_2=1.5$ are shown in Fig. 5, for a range of detuning frequencies $\Omega$. Integration of $w(t)$ over all time for a range of $\Omega$ gives the line shapes (disregarding effects of the slowly varying momentum matrix elements) shown in Fig. 6, for a range of damping ratios. For small damping, $\tau_0/T_2<1$, the line shape is fit approximately by $\operatorname{sech}^2(\pi\Omega\tau_0/2)$, i.e., the squared Fourier transform of the driving field, and the half width varies as $1/\tau_0$. For larger damping, the line shape becomes Lorentzian with half

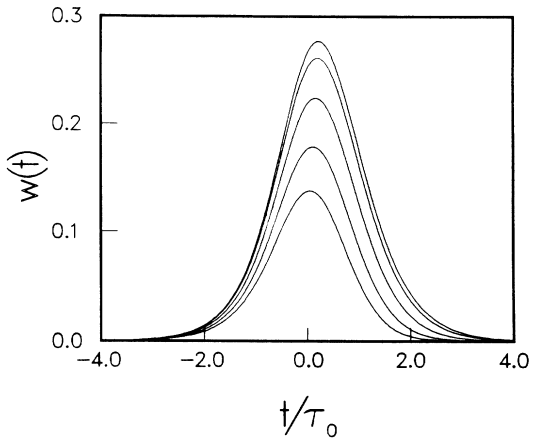


FIG. 5. Time-dependent absorption transition rate $w(t)$, for fixed $\tau_0/T_2=1.5$. From top to bottom, the curves correspond to values of the detuning frequency $\Omega\tau_0$ of 0, 0.5, 1.0, 1.5, and 2.0. Note that while $t=0$ corresponds to the center of the laser pulse, $w(t)$ peaks slightly after $t=0$, depending on the damping and detuning.

width $1/T_2$. For most cases considered here, with a laser intensity pulse with FWHM equal to 100 fs, such that $\tau_0=28.4$ fs, the transitions will be heavily damped. For example, for the transitions from the heavy-hole band, the damping time $T_2$ can be around 10 fs, producing a FWHM up to about 120 meV. Low damping will occur only for photon energies just above 1.44 and 1.77 eV, where transitions into states near $\mathbf{k}=0$ take place. Then the effective damping time $T_2\approx 370$ fs when there is no field.

For low enough damping, $\tau_0/T_2<1.3$, the time-dependent transition probability $w(t)$ can be negative a short time after $t=0$. This corresponds to stimulated emission immediately following the absorption. For a time-dependent simulation at time scales shorter than the laser pulse width, this would complicate the algorithm for creating electron-hole pairs, because we would also need to allow for the stimulated recombination process.

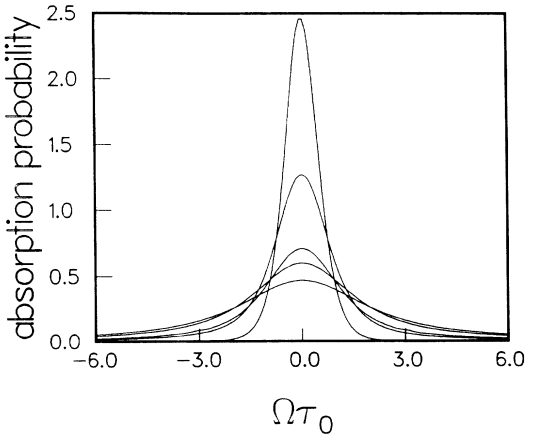


FIG. 6. Absorption line-shape functions, as obtained by integration of $w(t)$ over all time. From top to bottom, the curves correspond to values of the daming ratio $\tau_0/T_2$ of 0, 0.5, 1.0, 1.5, and 2.0. The line shape changes from a squared hyperbolic secant to a Lorentzian for $\tau_0/T_2$ greater than about 1.3.

For the simulations presented here this is not a problem because the response well after the light pulse is desired, and the pairs can be thought of as being created almost simultaneously. The recombination can be treated in terms of negative weights for the trajectories of electron-hole pairs that were created when $w<0$. For most cases only the transition from the split-off band will have such low damping, for a 100-fs pulse. Such transitions contribute the smallest number of electrons to the conduction band. (See Fig. 4.)

The damping time $T_2$ is determined as follows. The damping *rate* $1/T_2$ should have a contribution $1/\tau_{\text{scatt}}$ due to the total scattering rate of the electron, plus a contribution due to drifting in the applied field, written in terms of a drift time as $1/\tau_{\text{drift}}$,

$$\frac{1}{T_2}=\frac{1}{\tau_{\text{scatt}}}+\frac{1}{\tau_{\text{drift}}} . \tag{19}$$

The drift time $\tau_{\text{drift}}$ is taken to be the average time interval needed for the electron to drift in the applied field across the half width at half maximum (HWHM) of the absorption line, according to the semiclassical equation of motion

$$\frac{1}{\tau_{\text{drift}}}=\frac{eE}{\hbar\Delta k}=\frac{eE}{\Delta\varepsilon}\left[\frac{1}{\hbar}\frac{\partial\varepsilon}{\partial k}\right] . \tag{20}$$

Here $\Delta\varepsilon$ is the HWHM of the absorption line. The product $\tau_0\Delta\varepsilon$ is a function only of $\tau_0/T_2$. Thus $\tau_{\text{drift}}$ can be eliminated from Eqs. (19) and (20), and we can solve for $T_2$ numerically, with the help of the known relationship for the HWHM as a function of $\tau_0/T_2$. (See Fig. 6.) In this way the drift time $\tau_{\text{drift}}$ and the HWHM are determined self-consistently, even when the scattering time becomes much larger than $\tau_0$. The drift times varies as the reciprocal square root of the applied field. For example, if $\tau_{\text{scatt}}\gg\tau_0\gg\tau_{\text{drift}}$, then one obtains $T_2\approx\tau_{\text{drift}}$, with

$$\tau_{\text{drift}}^2=\frac{\hbar(1+2\alpha\varepsilon)}{eE}\left[\frac{m^*}{2\varepsilon(1+\alpha\varepsilon)}\right]^{1/2} . \tag{21}$$

Here $\varepsilon$ is the energy measured from the bottom of the valley. This formula applies most accurately at high field. For example, with $E=30$ kV/cm and for a transition from the split-off band with a 100-fs pulse of 1.55-eV photons, $\varepsilon=0.1$ eV, and Eq. (21) gives $\tau_{\text{drift}}\approx 18$ fs. When the above inequalities are not satisfied, $\tau_{\text{drift}}$ needs to be determined numerically.

Distributions of initial states from photoexcitation are shown in Figs. 7 and 8, for GaAs at photon energies of 1.5 and 2.0 eV, respectively, as a function of the angle $\theta$ measured from the [001] direction as in standard spherical coordinates. Initial states out to 5% of the maximum of the absorption line were included in these figures. In part (a) of these figures no linewidth was included; an energy width still results because of the anisotropy of the valence bands. In part (b), the width due to scattering, a laser pulse with a 100-fs FWHM, and no electric field was included. In part (c), the width due to scattering, the laser pulse, and a 10-kV/cm field was included. The individual contributions from the split-off, light-hole, and

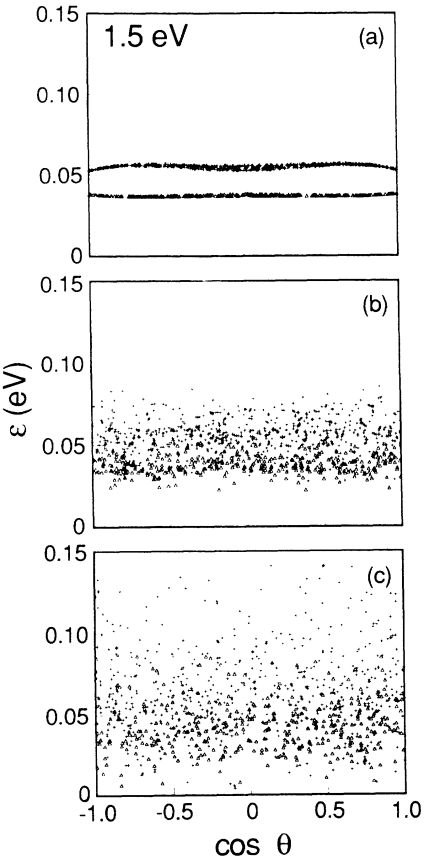


FIG. 7. Photo-induced initial-state energies as a function of polar angle $\theta$ for 1.5-eV photons. Here and in Fig. 8, the symbols indicate contributions from the split-off (○), light-hole (△), and heavy-hole (+) valence bands. In (a) no linewidth is included. In (b), the linewidth due to a 100-fs laser pulse combined with that due to finite $T_2$ is included. (c) is the same as (b) but with the addition of a 10-kV/cm field.

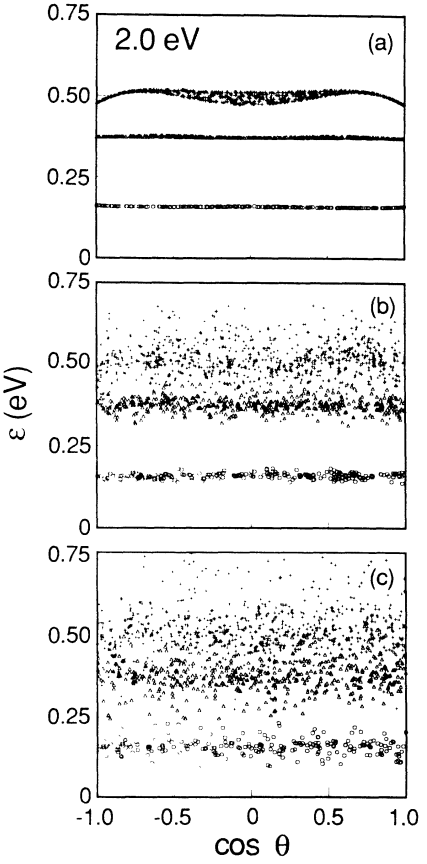


FIG. 8. Photo-induced initial-state energies as a function of polar angle $\theta$ for 2.0-eV photons, with (a), (b), and (c) as described in Fig. 7.

heavy-hole valence bands are (most obvious when the linewidths are not included) indicated by the symbols ○, △, and +, respectively. The linewidths increase with the photon energy due to the increase of the scattering rates with energy. They also increase as the field increases, due to the reduction of the drift time $\tau_{\text{drift}}$. Another representation of the distribution of states generated by the light field is given in Figs. 9 and 10, in terms of the number as a function of the conduction-band energy. Note that the states represented in Figs. 7–10 involve transitions at arbitrary times [the transition rate $w(t)$ has been integrated over time to obtain these results], and so these plots *do not* represent the distribution function at $t=0$. They are used only to indicate what initial states are possible for the given energy and electric field, with the creation time of an electron into one of these states being undetermined.

The weighting of the trajectories is a function of the polarization of the light. Nevertheless, we have not found any strong dependence of the transition responses on the polarization in the MC calculations. As suggested above, for time scales of the order of $\tau_0$, the effects of the

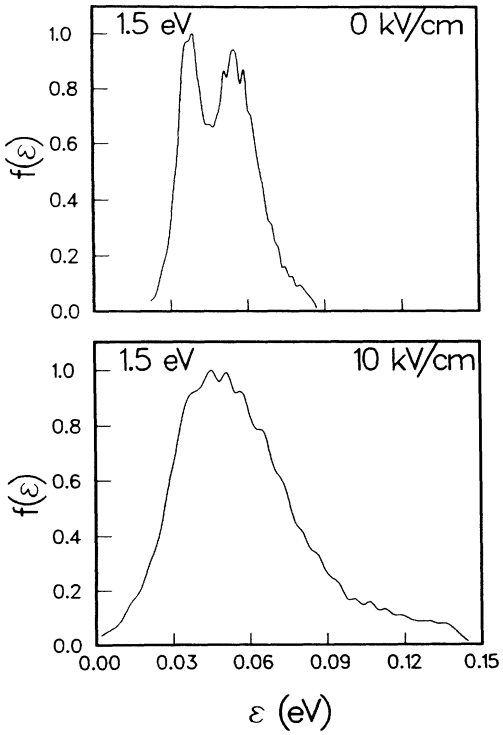


FIG. 9. Conduction-band energy distribution of the photoexcited electrons with 1.5-eV photons, for no field and 10 kV/cm.

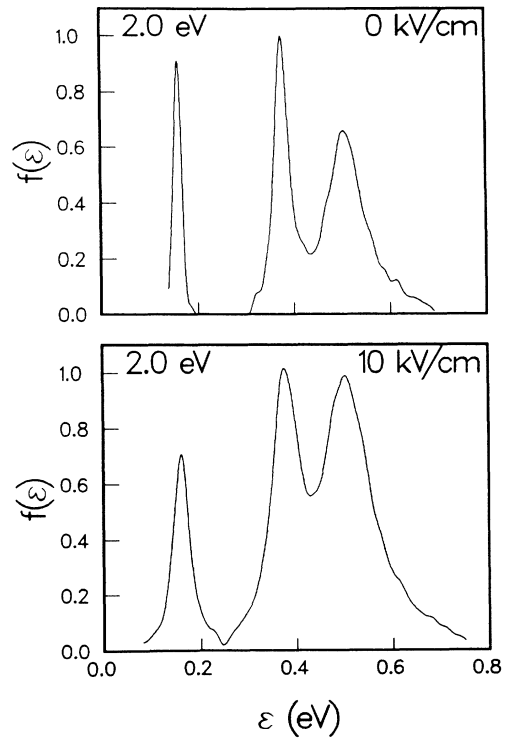


FIG. 10. Conduction-band energy distribution of the photoexcited electrons with 2.0-eV photons, for no field and 10 kV/cm.

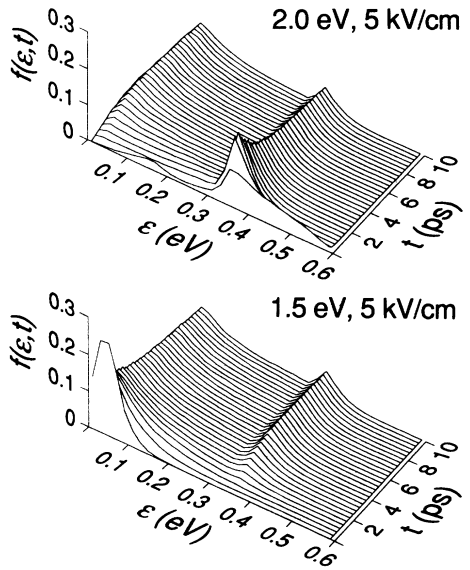


FIG. 11. Evolution of an energy-distribution function for an example without velocity overshoot (2.0 eV, 5 kV/cm) and one with velocity overshoot (1.5 eV, 5 kV/cm).

time-dependent part of $w(t)$ can be included by using a set of creation times appropriate to Eqs. (14)–(18), as chosen with a rejection probability technique.

## V. MONTE CARLO TRANSIENT RESULTS AND DISCUSSION

Calculations were made for photoexcitation by a laser pulse whose intensity has a FWHM of 100 fs, corresponding to $\tau_0=28.4$ fs. The photon energies were 1.5, 1.7, 1.8, 2.0, and 2.2 eV. For $\hbar\omega_0<1.77$ eV, only the light-hole and heavy-hole bands contribute to the absorption. The electric field ranged from 2.0 to 50.0 kV/cm. For each case average values of the velocity, energy, valley populations, and distribution functions $f(\varepsilon)$ were computed, as functions of time. Calculations required between 1000 and 10 000 electrons in order to limit the statistical errors. For the data presented in Figs. 11–15, the light was polarized along [100], and the electric field was in the [100] direction. The responses exhibited only very slight dependences on the polarization and field directions.

Some typical time evolutions of the distribution function $f(\varepsilon)$ are shown in Fig. 11, for $\hbar\omega_0=1.5$ and 2.0 eV, and $E=5$ kV/cm. Note that the earliest $f(\varepsilon)$ exhibited is slightly after the center of the laser pulse, and is not exactly the same as the curves in Figs. 9 and 10, which were time integrals of the transition rate. Although the initial distributions in Fig. 11 are different, both of them evolve to the same final distribution, which depends only on the applied field. The two peaks in the steady-state distribu-

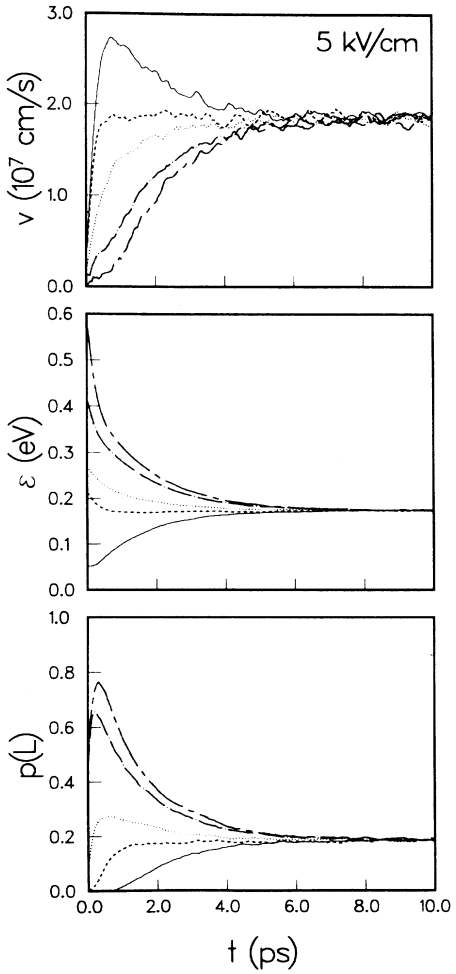


FIG. 12. Transient responses of the average velocity, average energy, and $L$-valley fractional population for a field of 5 kV/cm, with a 100-fs laser pulse (FWHM of the intensity). The curves correspond to photon energies 1.5 eV (——), 1.7 eV (— — —), 1.8 eV (· · · ·), 2.0 eV (—·—·—·), and 2.2 eV (—··—··).

tion correspond to the populations in the Γ and $L$ valleys, with about 20% in the $L$ valley. The lower graph (1.5 eV) corresponds to a case which exhibits velocity overshoot, where a sizeable fraction of the electrons are created at energies well below the steady-state average energy of 0.17 eV. Conversely, for 2.0 eV no velocity overshoot occurs, and a large fraction of the electrons are created well above the steady-state average energy.

A set of transient response curves are shown in Fig. 12 for a field of 5 kV/cm. The average electron velocity, average electron energy measured from the Γ minimum, and the fraction of the electrons in the $L$ valleys are shown as functions of time. The $X$ valleys are only slightly populated for most of the calculations shown here.[14] From top to bottom, the curves for average velocity correspond to the five photon energies, 1.5, 1.7, 1.8, 2.0, and 2.2 eV. Note that the order is reversed in the average energy and $L$-valley population graphs. The steady-state value of each quantity is independent of the photon energy. The transients, however, have a clear dependence on the photon energy. Only the 1.5-eV excitation produces an obvious velocity overshoot. The 1.7-eV excitation appears to be just over the maximum energy that will produce velocity overshoot. The higher proton energies do not produce an overshoot and exhibit a much longer velocity rise time. The average energy and $L$-valley population responses are correlated to the average velocity responses. The cases that exhibit velocity overshoot involve an average energy that increases with time. When no velocity overshoot occurs, the average energy monotonically decreases with time. The behavior of the population of the $L$ valley is similar to that of the average energy. When velocity overshoot occurs, the fractional $L$ valley population increases monotonically with time. On the other hand, when no velocity overshoot occurs, the $L$-valley population overshoots its steady-state value. The only exception to these observations might be for the 1.7-eV excitation, because it is so close to producing velocity overshoot.

A similar set of responses, for a field of 10 kV/cm, are shown in Fig. 13, for the same set of excitation energies. The time scale in this figure is shorter than in Fig. 12, and the steady-state values have changed, but the general relationships between the response quantities are the same. Now velocity overshoot occurs for the 1.5-, 1.7-, and 1.8-eV excitations, and these are the only cases with an increasing average energy transient, and a monotonically increasing $L$-valley population (or $L$-valley popula-

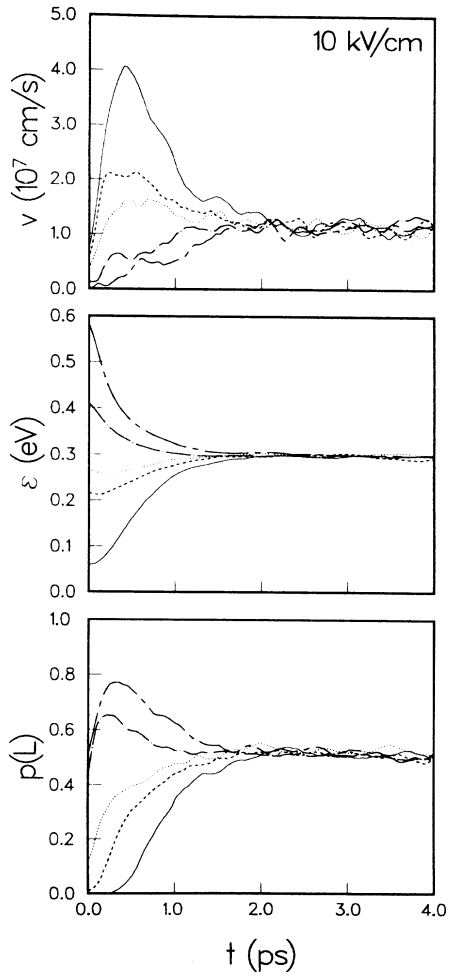


FIG. 13. Transient responses as described in Fig. 12, for a field of 10 kV/cm.

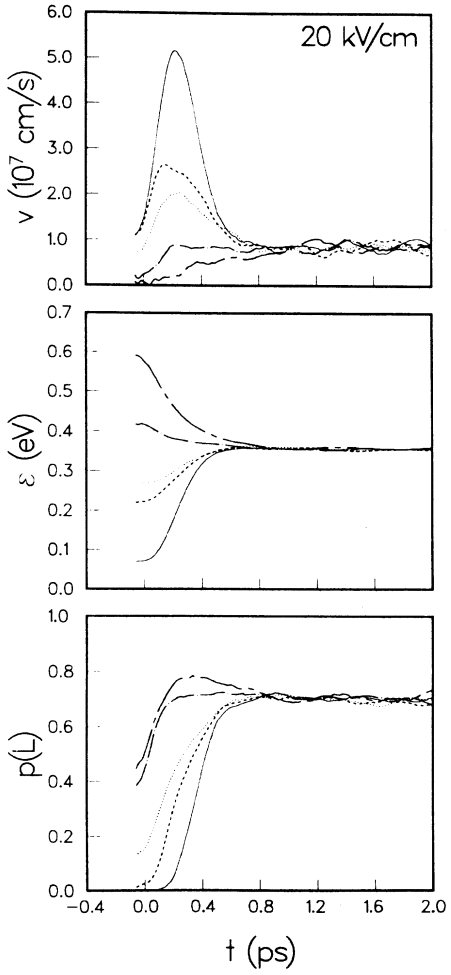


FIG. 14. Transient responses as described in Fig. 12, for a field of 20 kV/cm.

tion that does not overshoot). Also, it is clear that the relative size of the overshoot for 1.5 eV is now larger than it is for the 5-kV/cm field.

If the field is increased to 20 kV/cm, the responses shown in Fig. 14 are obtained. Note that again the steady-state values have changed, and the time scale of the graphs has been shortened. As the field is increased the average energy increases, causing the average scattering time to be reduced, and consequently shortening the response time. Now we see that the 2.0-eV excitation is very close to producing velocity overshoot. The correlations between the response quantities are the same as in Figs. 12 and 13.

Finally, a set of response curves for a field of 50 kV/cm is shown in Fig. 15. The 2.0-eV excitation appears to be very near the limit for overshoot. In the average energy response for 2.0 eV, there is initially a very small decrease followed by a small increase, the latter accounting for the velocity overshoot feature. At this field only the 2.2-eV excitation does not produce velocity overshoot. The $L$-valley population response for 2.2 eV, does not exhibit an overshoot as might be expected from the observations for the lower fields, because about 25% of the electrons transiently occupy the $X$ valleys (Ref. 14). The relative sizes of the velocity overshoots for excitations below 2.0 eV have increased well above those seen for 10 kV/cm.

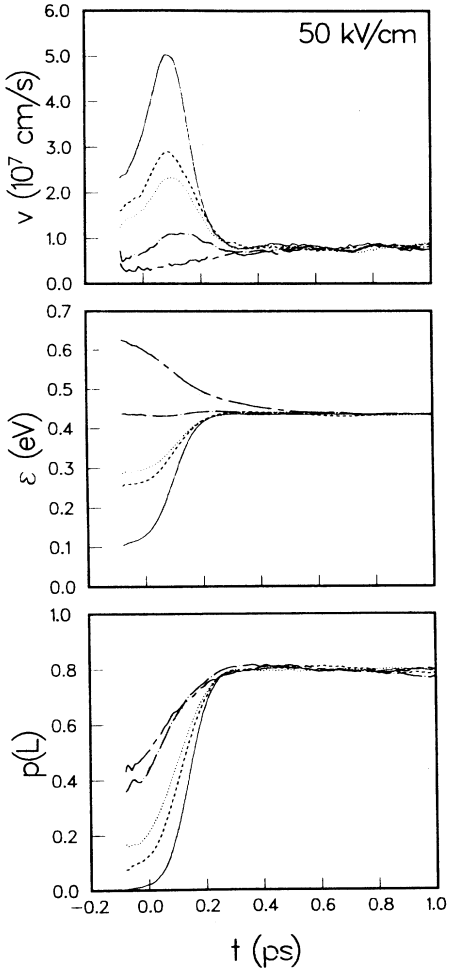


FIG. 15. Transient responses as described in Fig. 12, for a field of 50 kV/cm.

For all of these fields, any velocity overshoot features present at low $\hbar\omega_0$ eventually are suppressed at higher $\hbar\omega_0$. Also, a velocity overshoot is always accompanied by an increasing energy transient. Conversely, lack of overshoot is associated with a decreasing energy transient. This suggests that knowledge of the initial- and steady-state average energies generally is adequate to predict velocity overshoot. There may be a few exceptions where the photon energy is near the maximum for which velocity overshoot is allowed. These data make clear the idea of a critical field (or critical photon energy) necessary for overshoot.

These results can be summarized in terms of a photon energy—electric field "phase diagram." In particular, a curve can be drawn that corresponds to the photon energy needed so that the initial average electron energy $\varepsilon_i(\hbar\omega_0, E)$ is equal to the steady-state average energy $\varepsilon_{ss}(E)$, as from Fig. 3. Such a phase diagram is presented in Fig. 16. Individual cases tested are indicated on the diagram as either solid, for overshoot, or open, for no overshoot. One can see that the general rule is that all of the overshoot cases fall below the equi-energy curve described above. The question can be raised whether this rule will still be valid for other temperatures. A number of calculations were also performed for 77 K. It was found that the rule still generally holds, but there are some exceptions to it when the initial energy is just above the steady-state value, where overshoot can still occur. This happens because there is a very fast drop in the average energy, followed by a rise back towards the steady-state value, which is synchronized with the velocity overshoot feature.

The relative magnitude of the velocity overshoot is a function of both $\hbar\omega_0$ and $E$. This is exhibited in Fig. 17,

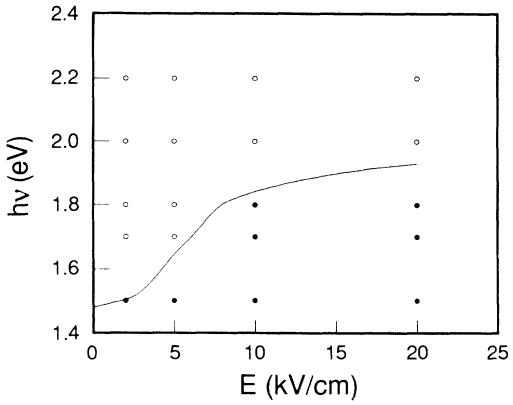


FIG. 16. Overshoot "phase diagram," in terms of the photon energy $h\nu$ and the field $E$. The solid circles represent simulations in which velocity overshoot occurred; the open circles represent cases where overshoot did not occur. The curve corresponds to cases where the steady-state average electron energy is equal to the average electron energy of the photoexcited electrons.

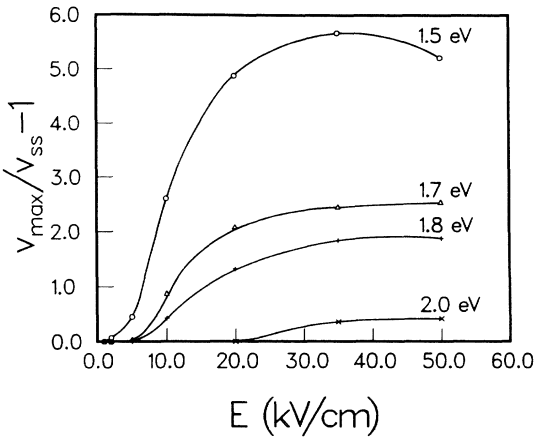


FIG. 17. Magnitude of velocity overshoot as a function of the applied field, in terms of the maximum average velocity $v_{max}$ and the steady-state average velocity $v_{ss}$.

in terms of the maximum velocity $v_{max}$ and the steady-state velocity $v_{ss}$, where the relative overshoot $(v_{max}-v_{ss})/v_{ss}$ is plotted versus the applied field for various photon energies. Critical turn-on fields can be seen; there is a tendency for the relative overshoot to saturate with increasing field.

Some transients at high photon energy also show another interesting feature, in cases where a large fraction of the electrons have been created high in the $\Gamma$ valley of the conduction band and then scatter very quickly ($< 10$ fs) into the $L$ valley. This dramatically reduces the effective mobility to such an extent that the velocity transient has a delay interval, where $v$ is very small before eventually beginning to slowly rise towards its steady-state value.

## VI. SUMMARY AND CONCLUSIONS

We have presented a systematic series of Monte Carlo calculations of electron relaxation in GaAs. The case was considered in which the electrons are generated by a 100-fs optical pulse and the GaAs is biased by a uniform-in-space and constant-in-time electric field. We investigated the dynamics of the electron relaxation as a function of the photon energy and the magnitude of the applied field. We have found that velocity overshoot occurs when the initial average electron energy is less than the steady-state value and does not occur when the opposite is true. In particular, for excitation with 2.0-eV photons, as occurs in experiments using direct excitation from a CPM laser, velocity overshoot does not occur for applied fields less than about 30 kV/cm. These results demonstrate the importance of using a spectrally tunable source in experiments designed to observe velocity overshoot.

## ACKNOWLEDGMENTS

This work was financially supported by the Defense Advanced Research Projects Agency and by Los Alamos National Laboratory Internal Supporting Research.

[1]C. Jacobini and L. Reggiani, Rev. Mod. Phys. **55**, 645 (1983).
[2]W. Fawcett, A. D. Boardman, and S. Swain, J. Phys. Chem. Solids **31**, 1963 (1970).
[3]J. G. Ruch, IEEE Trans. Electron Devices **ED-19**, 652 (1972).
[4]K. Brennan and K. Hess, Solid State Electron. **27**, 347 (1984).
[5]M. A. Littlejohn, J. R. Hauser, and T. H. Glisson, J. Appl. Phys. **48**, 4587 (1977).
[6]R. B. Hammond, Physica B+C **134B**, 475 (1985).
[7]G. Mourou, K. Meyer, J. Whitaker, M. Pessot, R. Grodin, and C. Caruso, in *Picosecond Electronics and Optoelectronics II*, Vol. 24 of *Springer Series in Electrophysics* (Springer-Verlag, Berlin, 1987).
[8]M. C. Nuss, D. H. Auston, and F. Capasso, Phys. Rev. Lett. **58**, 2355 (1987).
[9]A. M. Johnson and W. M. Simpson, Opt. Lett. **8**, 554 (1983).
[10]R. W. Schoenlein, W. Z. Lin, E. P. Ippen, and J. G. Fujimoto, Appl. Phys. Lett. **51**, 1442 (1987).
[11]A. E. Iverson and D. L. Smith, IEEE Trans. Electron Devices **ED-34**, 2098 (1987); A. E. Iverson, G. M. Wysin, D. L. Smith, and A. Redondo, Appl. Phys. Lett. **52**, 2148 (1988).
[12]K. Brennan and K. Hess, Phys. Rev. B **29**, 5581 (1984).
[13]M. L. Cohen and T. K. Bergstresser, Phys. Rev. **141**, 789 (1966).
[14]Appreciable $X$-valley populations occur *transiently* for photon energies larger than about 1.9 eV. This population is about 25% for 2.2-eV photons. Appreciable *steady-state* $X$-valley populations occur for fields above 30 kV/cm. At 50 kV/cm, about 5% of the electrons occupy the $X$ valleys.